

Fundamentals of Noble Gas Thermochronometry

T. Mark Harrison

*Research School of Earth Sciences
The Australian National University
Canberra, A.C.T. 0200, Australia
director.rses@anu.edu.au*

Peter K. Zeitler

*Department of Earth and Environmental Sciences
Lehigh University
Bethlehem, Pennsylvania 18015, U.S.A.
peter.zeitler@lehigh.edu*

INTRODUCTION

The ideal geochronometer would be a universally stable phase that quantitatively retains both parent and daughter isotopes. Though a few mineral systems such as zircon U-Pb dating come reasonably close to this ideal, most minerals are incompletely retentive of daughter-product nuclides under crustal conditions. The mechanisms by which the daughter product can be lost from minerals include dissolution–reprecipitation reactions (e.g., salt; Obradovich et al. 1982), recrystallization (e.g., micas undergoing deformation; Chopin and Maluski 1980), and diffusive loss (e.g., ^{40}Ar degassing of K-feldspar; Foland 1974). The latter mechanism is perhaps the most common source of discrepancy between a radiometric mineral date and the age of the rock from which it formed.

Geochronologists have learned to turn this non-ideal behavior to their advantage and we now understand that most mineral ages from exhumed crustal rocks act in effect as kinetic thermometers sensitive to geologically-induced thermal effects. Such apparent ages are a measure of the temperature range over which daughter product ceased to be lost from a crystal, with intracrystalline diffusion usually acting as the rate-limiting process.

Consider the case in which a mineral sample containing a radioactive parent element experiences a complex thermal evolution, possibly involving heating as well as cooling. Within the sample, daughter product is continually produced by radioactive decay and lost by diffusion at natural boundaries. Although random at the scale of an individual atom, both diffusion and radioactive decay are highly predictable processes over longer and larger scales involving many particles. Coupled with the strong temperature dependence of diffusion, the elegant mathematics of the production-diffusion relationship make it possible to recover information about the thermal history experienced by such a sample, simply by knowing the amount of daughter product remaining in the mineral following cooling, or even better, by knowing the distribution of daughter product within the mineral. If one can justify the assumption of a monotonic cooling history of simple form, it is possible to assign a specific temperature to a bulk mineral date. By interpolating between several such data, a good approximation of the cooling history can be obtained. In the case of thermal histories involving reheating, if sufficient constraints are available it can be possible to estimate the magnitude or duration of a thermal event. Because natural thermal variations may be too subtle to be revealed by the

interpolation method mentioned, the preferred method is to harness knowledge of the internal concentration distributions where possible (see Harrison et al. 2005). Collectively, such approaches are termed thermochronometry (or thermochronology) (Berger and York 1981). Since geodynamic processes alter the distribution of heat in the crust, the thermal record preserved as isotopic variations in minerals can provide valuable insights regarding timing and rates of tectonic and surficial processes.

The tendency for minerals to lose daughter isotope relative to its parent is due in part to the nature of the transmutations caused by radioactive decay. For example, all three forms of beta decay result in the conversion of the parent element into adjacent isobars, with either one extra (β^+) or one fewer (β^- , electron capture) proton. Thus ^{40}K (an alkaline metal) decays either to ^{40}Ca (an alkaline earth) or ^{40}Ar (an inert gas). Both daughter elements are geochemically incompatible in a host mineral that contains potassium as an essential structural constituent. In the case of the U-Th/He system, ^4He is produced by intermediate, radioactive daughter isotopes during the series decay of ^{238}U , ^{235}U , and ^{232}Th into isotopes of Pb. For both these noble-gas systems, incompatibility is enhanced by the inability of inert gases to chemically bond in silicates and so at elevated temperatures in the crust, Ar and He will tend to be lost from potassium- and uranium-bearing minerals, resulting in K-Ar and U-He ages much younger than that of mineral formation. Indeed, for most minerals, quantitative noble-gas retention occurs only in the outer $\sim 0.2\%$ of the Earth, explaining why ^{40}Ar is the third most abundant gas in the atmosphere (He is sufficiently light that it rapidly achieves escape velocity and is lost from the atmosphere on short timescales). In general we expect that under crustal conditions in minerals of appropriate chemistry, the K-Ar and U-Th/He decay systems will behave as diffusively controlled thermochronometers.

In this chapter we focus on the K-Ar and U-Th/He decay systems and show how thermochronological data can be understood using solutions to the radioactive decay and diffusion equations. We review the fundamental principles of noble gas thermochronology with the intention of providing a basic grounding for those new to the field. Recent developments and advances in the field are the main subject of this volume, and references to recent work and discussion about ongoing controversies can be found in the relevant chapters.

BASICS OF NOBLE-GAS GEOCHRONOLOGY

K-Ar and $^{40}\text{Ar}/^{39}\text{Ar}$ systematics and analysis

The general age equation is:

$$t = \frac{1}{\lambda} \ln \left(1 + \frac{D}{P} \right) \quad (1)$$

where D is the daughter product, P is the parent, λ is the decay constant, and t is age. Because ^{40}K decays to both ^{40}Ar and ^{40}Ca , we must modify the K-Ar age equation to account for the fact that only about one in ten ^{40}K decays yield ^{40}Ar . This is done by dividing the total decay constant for ^{40}K ($\lambda = 5.543 \times 10^{-10}/\text{yr}$) by the partial decay constants to the ^{40}Ar branch by electron capture to an excited state ($\lambda_e = 0.572 \times 10^{-10}/\text{yr}$) and electron capture to the ground state ($\lambda_e' = 0.0088 \times 10^{-10}/\text{yr}$) (see McDougall and Harrison 1999). Thus the branching ratio is:

$$\frac{\lambda}{\lambda_e + \lambda_e'} = 9.54 \quad (2)$$

Substituting this expression in Equation (1) yields:

$$t = \frac{1}{\lambda} \ln \left(1 + \frac{\lambda}{\lambda_e + \lambda_e'} \frac{{}^{40}\text{Ar}}{{}^{40}\text{K}} \right) = \frac{1}{\lambda} \ln \left(1 + 9.54 \frac{{}^{40}\text{Ar}}{{}^{40}\text{K}} \right) \quad (3)$$

where ${}^{40}\text{Ar}/{}^{40}\text{K}$ is the present ratio of radiogenic ${}^{40}\text{Ar}$ to ${}^{40}\text{K}$.

In the ${}^{40}\text{Ar}/{}^{39}\text{Ar}$ method, the sample to be dated is irradiated with fast neutrons to transform a proportion of the ${}^{39}\text{K}$ atoms to ${}^{39}\text{Ar}$ via the ${}^{39}\text{K}(\text{n,p}){}^{39}\text{Ar}$ reaction. Following irradiation, the sample is placed in an ultrahigh vacuum system and heated to fusion to release argon which is then isotopically analyzed in a mass spectrometer. Following correction of the measured Ar isotope ratios for argon isotopes produced by interfering neutron reactions and atmospheric Ar (assuming that non-nucleogenic ${}^{36}\text{Ar}$ is associated with ${}^{40}\text{Ar}$ in a ratio equivalent to the modern atmospheric value of ${}^{40}\text{Ar}/{}^{36}\text{Ar} = 296$), a radiogenic ${}^{40}\text{Ar}/{}^{39}\text{Ar}$ ratio is calculated. Because this ratio reflects the sample ${}^{40}\text{Ar}/{}^{39}\text{K}$ value, it is therefore proportional to age (see Eqn. 9 below). This is because ${}^{39}\text{Ar}$ is a measure of the amount of ${}^{39}\text{K}$ in the sample, and the ${}^{40}\text{K}/{}^{39}\text{K}$ ratio is essentially constant in nature (Humayun and Clayton 1997). Rather than determining the absolute dose of fast neutrons the sample has received during irradiation, a standard sample of accurately known K-Ar age is irradiated together with the unknown, and the age of the unknown is then derived by comparison with the ${}^{40}\text{Ar}/{}^{39}\text{Ar}$ of the flux monitor standard.

Thus to derive the ${}^{40}\text{Ar}/{}^{39}\text{Ar}$ age equation, we first rearrange Equation (3) in terms of ${}^{40}\text{Ar}$:

$${}^{40}\text{Ar} = {}^{40}\text{K} \frac{\lambda_e + \lambda_e'}{\lambda} [(\exp \lambda t) - 1] \quad (4)$$

The amount of ${}^{39}\text{Ar}$ that is produced from ${}^{39}\text{K}$ during neutron irradiation is given by:

$${}^{39}\text{Ar} = {}^{39}\text{K} \Delta \phi(E) \sigma(E) dE \quad (5)$$

where ${}^{39}\text{Ar}$ is the number of atoms of ${}^{39}\text{Ar}$ produced from ${}^{39}\text{K}$ in the sample, ${}^{39}\text{K}$ is the original number of atoms of ${}^{39}\text{K}$ present, Δ is the duration of the irradiation, $\phi(E)$ is the neutron flux at energy E , and $\sigma(E)$ is the neutron capture cross section at energy E for the ${}^{39}\text{K}(\text{n,p}){}^{39}\text{Ar}$ reaction. Combining Equations (4) and (5) we get:

$$\frac{{}^{40}\text{Ar}}{{}^{39}\text{Ar}} = \frac{{}^{40}\text{K}}{{}^{39}\text{K}} \frac{\lambda_e + \lambda_e'}{\lambda} \frac{[(\exp \lambda t) - 1]}{\Delta \int \phi(E) \sigma(E) dE} \quad (6)$$

We then define the irradiation parameter, J , as:

$$J = \frac{{}^{39}\text{K}}{{}^{40}\text{K}} \frac{\lambda}{\lambda_e + \lambda_e'} \Delta \int \phi(E) \sigma(E) dE = \frac{(\exp \lambda t) - 1}{{}^{40}\text{Ar}/{}^{39}\text{Ar}} \quad (7)$$

If the age of a standard is known from K-Ar age measurements, then J can be determined from Equation (7) by simply measuring the ${}^{40}\text{Ar}/{}^{39}\text{Ar}$ ratio of the standard following irradiation. Substituting Equation (7) in Equation (6) gives:

$$\frac{{}^{40}\text{Ar}}{{}^{39}\text{Ar}} = \frac{(\exp \lambda t) - 1}{J} \quad (8)$$

Thus the ${}^{40}\text{Ar}/{}^{39}\text{Ar}$ age of an unknown is:

$$t = \frac{1}{\lambda} \ln \left(1 + J \frac{{}^{40}\text{Ar}}{{}^{39}\text{Ar}} \right) \quad (9)$$

Note from Equation (9) that the ratio of daughter ${}^{40}\text{Ar}$ to parent ${}^{40}\text{K}$ (via the ${}^{39}\text{Ar}$ proxy) is

measured in a single isotopic analysis, obviating the need for separate analyses of potassium and argon and thus overcoming problems of sample inhomogeneity. Another advantage is that an $^{40}\text{Ar}/^{39}\text{Ar}$ ratio can be measured more precisely and on smaller samples than a conventional K-Ar age. However, the major advantage of the $^{40}\text{Ar}/^{39}\text{Ar}$ method over the K-Ar method is that an irradiated sample can be heated in steps, starting at relatively low temperatures and eventually reaching fusion, permitting a series of apparent ages related to the gas released at that step to be determined on a single sample. This approach, known as the step-heating technique, provides a wealth of additional information that can provide insights into the distribution of ^{40}Ar in the sample relative to the distribution of ^{39}K (and thus ^{40}K).

In the ideal case, release of the argon in the vacuum system occurs by diffusion as the sample is progressively heated. Thus, for a sample that has retained its ^{40}Ar since crystallization, both ^{40}Ar and ^{39}Ar likely occur in similar lattice sites as they have both been derived from potassium (Fig. 1). If the two isotopes have similar transport behavior, they will be degassed in similar proportions thus yielding an essentially constant $^{40}\text{Ar}/^{39}\text{Ar}$ ratio and age in each gas fraction extracted. A plot of the apparent $^{40}\text{Ar}/^{39}\text{Ar}$ age for each step against cumulative proportion of ^{39}Ar released (termed an “age spectrum”) will yield a flat release pattern called a plateau (Fig. 1a). However, a sample that has lost some of its ^{40}Ar , either during protracted residence at high temperature in the deep crust or during a thermal excursion, will have sites within its lattice that have different ratios of daughter ^{40}Ar to parent ^{40}K . During a step-heating experiment, such differences may be revealed by variations in the $^{40}\text{Ar}/^{39}\text{Ar}$ ratio measured on the gas fractions successively released from the sample, yielding a staircase-type age spectrum (Fig. 1b,c).

In principle, any potassium-bearing mineral or rock can be used for K-Ar or $^{40}\text{Ar}/^{39}\text{Ar}$ dating. In practice, dateable samples are limited to those in which potassium is an essential

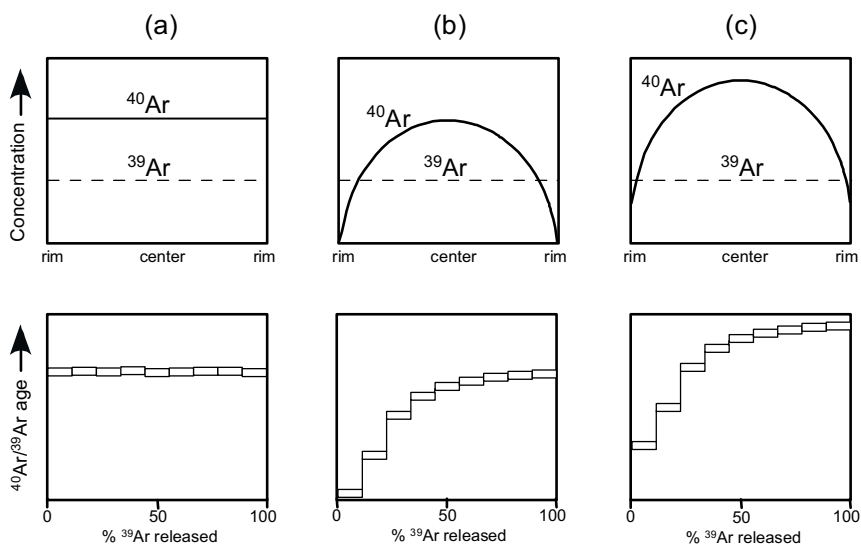


Figure 1. The top diagram portrays the concentration of ^{40}Ar and ^{39}Ar across an idealized mineral, and the lower diagram shows the associated $^{40}\text{Ar}/^{39}\text{Ar}$ age spectrum. a) Undisturbed subsequent to initial crystallization and rapid cooling yields a flat age spectrum; (b) diffusive loss of ^{40}Ar in recent times; (c) diffusive loss of ^{40}Ar during an ancient event with subsequent uniform accumulation of ^{40}Ar . The age of the diffusion loss event is given by the intercept at 0% ^{39}Ar release and a minimum age for crystal formation by the last measured age (after McDougall and Harrison 1999).

structural constituent, such as micas and feldspars. Because the method is based upon the accumulation of radiogenic ^{40}Ar ($^{40}\text{Ar}^*$), the radiogenic signal becomes greater with increasing age, and therefore there is no older limit for the method. The main limitation occurs when the relative proportion of $^{40}\text{Ar}^*$ to total ^{40}Ar in a sample tends to zero. As this ratio decreases, the error in its measurement will increase exponentially and come to be quite sensitive to analytical limitations (see McDougall and Harrison 1999).

$^{40}\text{Ar}/^{39}\text{Ar}$ mineral thermochronometers

White micas. White micas typically contain high (8–10%) potassium concentrations and occur widely in peraluminous granitoids and metamorphic rocks (e.g., they are common in metapelites ranging from chlorite to ultra-high pressure facies). Muscovite is retentive of radiogenic Ar below $\sim 400^\circ\text{C}$ (Purdy and Jäger 1976) and is generally less susceptible to contamination by uptake of excess radiogenic Ar than biotite. Phengite, however, often contains excess argon (e.g. de Jong 2003). Unlike biotite, muscovite and phengite commonly yield $^{40}\text{Ar}/^{39}\text{Ar}$ age spectra that can be interpreted in terms of distribution of radiogenic Ar in the crystals, as the intracrystalline distribution of ^{40}Ar appears to be retained during vacuum step heating.

Biotite. Biotite is virtually ubiquitous in granitoid rocks and common in medium to high-grade metapelites. Its typically high (7–8%) potassium content makes it a common candidate for K-Ar analysis, although it generally contains relatively high atmospheric Ar contents. Its retentivity for Ar is somewhat less than that of muscovite. While a biotite $^{40}\text{Ar}/^{39}\text{Ar}$ age will approximate the age of emplacement in the case of rapidly cooled igneous rocks, biotite ages from more slowly cooled igneous and metamorphic rocks will generally reflect the time of cooling. The inability to produce meaningful age spectra from biotites appears to result from its instability during heating *in vacuo*, which tends to destroy radiogenic-Ar diffusion gradients (McDougall and Harrison 1999).

K-feldspar. Because of their abundance in nature, especially in silicic rocks, and because of their relatively high potassium contents (up to 17%), alkali feldspars have been increasingly used for $^{40}\text{Ar}/^{39}\text{Ar}$ dating (e.g., Lovera et al. 1989), despite once being viewed as unretentive of argon at room temperature (Faure 1977). K-feldspar is the most prevalent potassium-rich silicate in the crust that is sufficiently stable during *in vacuo* heating to provide a reasonable expectation that natural $^{40}\text{Ar}^*$ diffusion properties could be reproduced in laboratory step-heating experiments (Fitz Gerald and Harrison 1993). Although the overall retentivity of K-feldspar for $^{40}\text{Ar}^*$ is typically lower than that of the micas, its characteristically complex microstructure results in a broad temperature range for partial argon retention. Because of its stability during *in vacuo* heating, K-feldspar is able to record nearly continuous thermal histories under middle to upper crustal conditions (Harrison et al. 2005).

Amphibole. Amphiboles are common in calc-alkaline igneous and metabasic rocks but are somewhat limited in K-Ar dating due to typically low (0.3–1%) potassium contents which make them susceptible to contamination with excess Ar or intergrowths with less retentive K-rich phases such as biotite (see McDougall and Harrison 1999). Hornblende is highly retentive of radiogenic Ar (Harrison 1981), although there appear to be a compositional dependence on Ar retention. The presence of fine-scale exsolution in metamorphic amphiboles, particularly involving micaceous phases, can have a significant effect on Ar retention in amphiboles.

Principal interpretive methods and analytical issues, $^{40}\text{Ar}/^{39}\text{Ar}$

The age spectrum. As shown in Figure 1, plotting $^{40}\text{Ar}/^{39}\text{Ar}$ age as a function of cumulative ^{39}Ar release can in theory create a representation of the intracrystalline distribution of radiogenic Ar. Such a diagram is known as an age spectrum. Assuming that Ar is transported solely by diffusion and that ^{40}Ar and ^{39}Ar originate from similar sites and diffuse at similar rates, we can derive a simple quantitative model that predicts the age spectrum for a given

internal distribution of ^{40}Ar (Fig. 5). Thus for a uniform distribution of ^{40}Ar , the model predicts a uniform $^{40}\text{Ar}/^{39}\text{Ar}$ ratio throughout the laboratory degassing process and a flat age spectrum is interpreted as a closed system since formation (Turner 1968). In many cases, notably the biotite micas, other possible degassing mechanisms (e.g., structural breakdown) dominate, potentially leading to flat age spectra in cases where initially heterogeneous $^{40}\text{Ar}/^{39}\text{Ar}$ distributions are homogenized (McDougall and Harrison 1999). It is also important to keep in mind that the values plotted on an age-spectrum diagram are not equivalent to a directly sampled concentration profile across a mineral: both the measured ^{40}Ar and ^{39}Ar have been released from the sample by progressive diffusion; indeed, age spectra will always tend to reach apparent plateaus late in the gas release as diffusion brings the ^{40}Ar and ^{39}Ar concentration profiles within the sample into similar forms.

Despite these cautions, for several years the practice of using the flatness of an age spectrum to distinguish between undisturbed and disturbed systems became unfortunately widespread, with any number of *ad hoc* definitions being proposed for what constitutes a plateau and therefore a “good” sample (see discussion in McDougall and Harrison 1999, p. 111). From a thermochronological perspective (as we will show below), a simple rule is that a sample exhibiting a flat release pattern will at best be boring, at worst be misleading, and in any case be of little use.

Total-fusion age. As an alternative to step-heating analysis, which can be quite time-consuming, one has the option of measuring the total gas content of a sample in a single step. The result is termed a total-fusion age, and is equivalent to the sample’s conventional K-Ar age. This approach would be inadvisable for samples having recoverable diffusion information, but certainly in the case of biotite, which is notorious for yielding false plateaus even in cases where the mineral must contain diffusion-produced concentration gradients, the argument could be made that for equivalent cost and effort, analysis of a greater number of discrete samples far outweighs any benefits gained by step-heating.

Excess argon. The K-Ar method routinely assumes that all mineral samples are contaminated with non-radiogenic Ar, albeit with Ar of atmospheric composition as noted above. However, this will only be the case if the minerals’ immediate surroundings represent a more compatible reservoir for Ar than the host phase (see Baxter et al. 2002). Thus in certain cases, samples can be contaminated with non-radiogenic Ar that greatly exceeds the atmospheric $^{40}\text{Ar}/^{36}\text{Ar}$ ratio resulting in anomalously old ages that in some cases exceed that of the Earth (Pankhurst et al. 1973; Harrison and McDougall 1981). Early on, it was believed that many age spectra thus contaminated were characterized by “saddle-shaped” behavior, in which high initial ages decrease to a minimum and then rise to high apparent ages in the last portion of the gas release. The high ages early in gas release were thought to be due to diffusive uptake of excess Ar ($^{40}\text{Ar}_E$) from a high P_{Ar} reservoir exterior to the grain with the minimum ages yielding an estimate of the true age. Harrison and McDougall (1981) suggested that the anomalously old ages late in release were due to excess Ar trapped in retentive lattice sites. It was subsequently noted that feldspars degassed using duplicate isothermal steps yielded saw-toothed age patterns (Harrison et al. 1993) that reflect decrepitation of Ar_E -bearing fluid inclusions. By linking the saw-tooth age pattern with Cl/K ratios calculated from nucleogenic Ar isotopes, a correction scheme can be devised permitting separation of $^{40}\text{Ar}_E$ from *in situ* radiogenic ^{40}Ar , at least for feldspars (Harrison et al. 1994).

Recoil. While we assume that the ^{39}Ar produced from ^{39}K during irradiation is distributed in a manner similar to the ^{40}K in a sample, the $^{39}\text{K}(n,p)^{39}\text{Ar}$ reaction results in ^{39}Ar nuclei being recoiled with a characteristic lengthscale of 0.08 μm (Turner and Cadogan 1974). Ultra-fine grained samples, such as clays or lunar basalts, exhibit effects of recoil redistribution of ^{39}Ar and can yield highly complex age spectra owing to depletion of ^{39}Ar from some phases and

implantation into retentive catcher phases like olivine (Huneke and Smith 1978). However, age spectra of the type routinely used in thermochronometry (i.e., monomineralic separates with particle dimensions much greater than the recoil distance) are unlikely to be affected by recoil redistribution. Note however, that the characteristic recoil lengthscale of 0.08 μm limits the spatial resolution of diffusion studies of irradiated material to $\sim 0.1 \mu\text{m}$.

(U-Th)/He systematics and analysis

Shortly after the discovery of radioactivity, it was recognized that the accumulation of ^4He from U and Th α -decay could be used as a geochronometer (e.g., Strutt 1908). By the 1950's, however, it was generally recognized that most minerals were extremely "leaky" for He and the approach was essentially abandoned (Hurley 1954) until the method was re-evaluated from a thermochronological perspective (Zeitler et al. 1987).

In the minerals of greatest relevance to thermochronology, ^4He and several Pb isotopes are the stable products of the ^{238}U , ^{235}U , and ^{232}Th decay series (^4He production from ^{147}Sm decay is usually negligible). The equation for ^4He accumulation is:

$$^4\text{He}_{\text{all}} = 8 \left(\frac{137.88}{(1+137.88)} \right) C_{\text{U}} (e^{\lambda_{238}t} - 1) + 7 \left(\frac{1}{(1+137.88)} \right) C_{\text{U}} (e^{\lambda_{235}t} - 1) + 6 C_{\text{Th}} (e^{\lambda_{232}t} - 1) \quad (10)$$

where C_{U} and C_{Th} are, respectively, the concentrations of uranium and thorium, λ_{238} ($1.55125 \times 10^{-10} \text{ yr}^{-1}$), λ_{235} ($9.8485 \times 10^{-10} \text{ yr}^{-1}$), and λ_{232} ($4.9475 \times 10^{-11} \text{ yr}^{-1}$) are the relevant U and Th decay constants, and t is age. The expression, which can be solved recursively for age using the Newton-Raphson method, assumes secular equilibrium within the ^{238}U , ^{235}U , and ^{232}Th decay chains. This condition is met provided the host mineral is older than ca. 350 ka; in the case of petrologically old but very recently exhumed samples giving very young He ages, secular equilibrium in the decay series will long ago have been established, the young age being a reflection of ^4He loss, not decay-series parents.

Unlike $^{40}\text{Ar}/^{39}\text{Ar}$ dating, which is generally applied to rocks and minerals containing the major element potassium, U-Th/He dating involves analysis of accessory minerals in which the radioactive parent elements uranium and thorium are concentrated, but nevertheless present in only trace amounts. Several factors combine to leave helium dating a viable method. First, the lower abundances of U and Th relative to K are to some degree offset by the faster effective production of He compared to Ar: for a given concentration of parent, more than 20 times more ^4He is produced per decay of ^{238}U than ^{40}Ar per decay of ^{40}K . Next, while the noble gases have impressively low detection limits in general, the measurement of even small amounts of ^4He is straightforward and not complicated by isobaric interferences from hydrocarbons as can be the case for Ar isotopes. Finally, of greatest significance is that background levels of He in the atmosphere are very low, on the order of 1 ppm, compared to the $\sim 1\%$ of air that is ^{40}Ar . Thus, He ages do not require correction for an atmospheric component. In the considerable number of studies carried out in recent years, there is little evidence that geologically trapped, "excess" ^4He is an issue. However, ^4He is a crustal component that can locally reach high concentrations (e.g., gas wells) and there may be certain environments (e.g., active shear zones, fluid inclusions) in which excess ^4He may be present. In any event, given the great range in observed $^4\text{He}/^3\text{He}$ ratios, the magnitude of this ratio ($\sim 10^6$), and the low abundance of natural ^3He , it would not be realistic to attempt corrections for trapped ^4He in the way that Ar ages are corrected for atmospheric Ar, and fortunately atmospheric contamination does not appear to be a problem.

Most laboratories today analyze for ^4He using vacuum extraction systems similar to that used for $^{40}\text{Ar}/^{39}\text{Ar}$ dating. Samples are heated in either a furnace or by laser, the released gases are purified, a ^3He spike is added, and the resulting mixture analyzed, in most cases by an inexpensive quadrupole mass spectrometer. Step-heating analysis is possible for the

purpose of determining diffusion data from the release of ^4He , but there is no way to generate a reference helium isotope from U and Th in the way that ^{39}Ar is used in $^{40}\text{Ar}/^{39}\text{Ar}$ dating, and so age spectra cannot be measured. One practical matter unique to helium step-heating analysis is that the low-temperatures at which He is released from some minerals make the traditional double-vacuum furnaces used in many noble-gas laboratories inappropriate, as these furnaces are too slow to equilibrate at these temperatures. Instead, special furnaces need to be constructed that are more responsive at low temperature, like the projector-bulb system described by Farley et al. (1999).

(U-Th)/He mineral thermochronometers

Apatite. Apatite is the principal host of phosphorus in crustal rocks and is therefore virtually ubiquitous. Apatite typically contains 2–20 ppm U and, as other phosphates, tends to anneal radiation damage at low temperatures making it an appealing mineral for (U-Th)/He dating. Ironically, what makes apatite particularly interesting is the characteristic that led to the approach being abandoned in the middle 20th century—the purported “leakiness” of He in minerals. In revisiting applications of (U-Th)/He dating, Zeitler et al. (1987) focused on apatite as a phase likely to be unretentive of He. They proposed a “closure temperature” (see discussion below) of He in apatite of about 100 °C which was subsequently refined by further diffusion measurements to ~70 °C (Farley et al. 1996, 2002; Wolf et al. 1996). This temperature is substantially lower than all other thermochronometers and thus has the greatest sensitivity to changes occurring at the Earth’s surface.

Zircon. Zircon is a very common accessory mineral found in most rock types, and the mineral has seen a great deal of use in geochronology, for U-Pb dating of high-temperature and rock-forming events, for provenance and protolith studies in sedimentary and metamorphic rocks, and for thermochronological studies using fission-track dating. Zircons typically contain 100’s to 1000’s of ppm of U and Th, and thus even very young zircons contain abundant ^4He . Zircon is more retentive of He than apatite (Reiners et al. 2002) and appears to overlap the retentivity of K-feldspar for Ar (Reiners et al. 2004).

Titanite (sphene). Titanite is another accessory mineral, fairly common in calc-alkaline igneous and metamorphic rocks, that contains 10’s to 100’s of ppm of U and Th. Work by Reiners et al. (1999) and Stockli and Farley (2004) have shown that titanite can give reliable and consistent ages, with the mineral having a retentivity for ^4He roughly on par with that of zircon. One drawback associated with titanite is that natural crystals often have irregular shapes that make it hard to identify fractured grains and hard to determine recoil-correction factors (see below).

Principal interpretive methods and analytical issues, (U-Th)/He

Bulk age. All helium ages are bulk ages that reflect the total integrated ^4He content of the sample. Work is underway to develop means of sampling He concentration gradients, but currently and for the immediate future, helium ages will be equivalent to K-Ar or total-fusion $^{40}\text{Ar}/^{39}\text{Ar}$ ages.

$^4\text{He}/^3\text{He}$ spectra. Shuster et al. (2003) and Shuster and Farley (2003) describe a means of assessing ^4He diffusion kinetics in the context of a uniform distribution of ^3He , somewhat analogous to how ^{40}Ar diffusion can be referenced to that of ^{39}Ar . A crucial difference is that the ^3He is produced via spallation using proton bombardment. Because most of the major elements in the sample will serve as targets, the ^3He that is produced will tend to be uniformly distributed. However, there is no possibility of obtaining age information because the spallation helium is not produced from the U and Th that are the parents for the radiogenic ^4He in the sample. Though technically more challenging, this approach does show some promise in providing information about ^4He concentration gradients that will be difficult if not impossible

to sample directly with laser techniques, given the fine spatial scale of microns over which these gradients are likely to exist.

Alpha (α)-recoil. A potentially serious complication inherent to (U-Th)/He dating is that the kinetic energy imparted to α -particles during decay result in their being displaced many microns through the host mineral, leading to a spatial separation between parent and daughter. In the case of minerals whose size is similar to the ejection length-scale, this can result in the ejection of a substantial fraction of the daughter ^4He . Typically, the outermost $\sim 20\ \mu\text{m}$ of a crystal is affected, the average alpha-particle range varying slightly depending on parent (Farley et al. 1996). The solution is to estimate the fraction of ejected ^4He and make a correction to the observed age (assuming that implantation from adjacent grains is insignificant and that U and Th are uniformly distributed). The most commonly used approach is that of Farley et al. (1996) who provide expressions to calculate the fraction of α -particles retained in crystals of varying geometry (the " F_T " parameter). Of practical significance, Farley et al. (1996) found that the key element in controlling alpha ejection is the surface-to-volume ratio, and they provide an empirical expression between this ratio and F_T , allowing corrections to be readily made for more complex grain geometries for which a simple analytical solution is not available.

The need to correct helium ages for recoil raises some analytical constraints and issues. First, it is important to analyze intact grains, unless pairs of broken grains can be matched, since the correction procedure assumes an intact grain, all of whose surfaces have experienced recoil loss. Next, in the strictest sense, correction for α -recoil is only applicable to samples that have cooled quickly and never lost helium. For samples that have experienced a complex cooling history, the concentration gradient induced near grain ages by the recoil process will modify the concentration profiles produced by diffusion and thus the rate of diffusion itself (Meesters and Dunai 2002a). However, this will be a small effect, and for most samples which spend the greatest part of their lives accumulating a full complement of helium subsequent to cooling, the recoil correction makes sense and yields a far more meaningful result than leaving the age uncorrected.

U and Th heterogeneity. U and Th distributions in accessory minerals tend to be complex. Zoning in apatite is not usually very strong but in zircon in particular, years of experience with U-Pb and fission-track dating have shown that zircons can display extremely complicated high-amplitude zoning variations that are not always of regular pattern and morphology (Meesters and Dunai 2002b). This can greatly complicate the recoil-loss behavior of a sample and render attempts at recoil correction almost worse than useless. Consider the case where a sample is strongly zoned such that a good fraction of its total U content is located within $20\ \mu\text{m}$ of grain edges. Much of the helium generated in such a sample will be ejected from it, and an alpha-recoil correction made on the assumption of uniform U distribution will be inadequate. In practice, this problem can sometimes be overcome using replicate analyses, although if grains in a sample all have similar zoning structure, even replication may not help. Hourigan et al. (2005) describe a method of characterizing zoning patterns in zircons in order to make more appropriate alpha-recoil corrections.

DIFFUSION

Background

In noble-gas geochronology, it is generally assumed that the phase of interest is immersed in an 'infinite reservoir' of zero daughter product concentration and that the rate-determining diffusion process is volume diffusion through the crystal lattice, as opposed, say, to grain-boundary diffusion along crystallographic structures. In this case, no issues related to chemical potential arise and simple concentration is the parameter of interest. Noble-gas diffusion obeys

Fick's First Law: the rate of transfer of mass per unit area is proportional to the concentration gradient (Fick 1855). It is worth noting that Fick's First Law applies to the aggregate behavior of many diffusing particles. In detail, any one particle could move randomly in any direction, but if there is a concentration gradient present, this locally random behavior will result in a net movement of particles down the diffusion gradient. As an example, imagine an immaculate house in autumn surrounded by a garden filled with fallen leaves. As people tramp into and out of the house, they will tend to bring a leaf or two with them, and leaves will flow in both directions. However, because at the start there were more leaves outside than inside, there will be a net flux of leaves into the house. Should the homeowner surrender in despair and not intervene, eventually the concentration of leaves inside and out would become equal, and there would be no net flow, even as leaves continue to enter and exit the house.

The diffusion equation. The general problem of unsteady-state diffusion within a solid involves the prediction of the concentration distribution $C(x,y,z)$ within a solid as a function of the space coordinates and time, t . To derive an equation that can be solved for $C(x,y,z,t)$, conservation of mass and Fick's first law are applied to a differential control volume. The resulting expression is the diffusion equation:

$$\frac{\partial C}{\partial t} = D \left(\frac{\partial^2 C}{\partial x^2} + \frac{\partial^2 C}{\partial y^2} + \frac{\partial^2 C}{\partial z^2} \right) \quad (11)$$

where D is the diffusion coefficient. Solutions of the diffusion equation can be obtained for a number of initial and boundary conditions covering simple concentration distributions and diffusion geometries (Crank 1975). For example, using coordinate transformations, Equation (11) can be modified to describe radial flow in a sphere (see McDougall and Harrison 1999) and solved for the case of a sphere of radius r with an initially uniform concentration, C_0 , held in an infinite reservoir of zero concentration. The concentration distribution (\mathcal{R}) is given by:

$$C = \frac{C_0 2r}{\pi \mathcal{R}} \sum_{n=1}^{\infty} \frac{(-1)^n}{n} \sin \frac{n\pi \mathcal{R}}{r} \times \exp \left(\frac{-n^2 \pi^2 D t}{r^2} \right) \quad (12)$$

Diffusion mechanisms

Atoms migrate within a solid through a series of random jumps between equilibrium lattice sites. Distortion of the lattice to permit a diffusion jump is affected via local thermal energy and thus the rate of diffusion increases with increasing temperature. Although the rate of this random migration is independent of chemical potential in dilute solutions, the presence of concentration differences results in a net flux down the gradient. When a boundary is encountered beyond which no return of the diffusing species is possible (e.g., the edge of the crystal, sub-grain planar defects), the randomizing process of diffusion results in the movement of mass from regions of high to lower concentration.

Four possible transfer mechanisms for atomic diffusion are possible (Fig. 2): an exchange of adjacent atoms, an atom moving into a neighboring vacant lattice

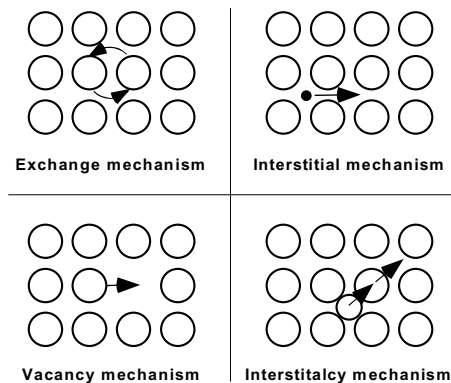


Figure 2. Schematic illustration of the four possible mechanisms of diffusion transport: Exchange, vacancy, interstitial, and interstitialcy.

While strongly dependent on temperature, diffusion is predicted to decrease as pressure increases due to both a drop in number of vacancies in response to the crystal relieving internal pressure and the extra work diffusing atoms must perform against the confining pressure to distort the lattice to make a diffusion jump. The modified Arrhenius equation is:

$$D = D_0 \exp\left(-\frac{(E + PV)}{RT}\right) \quad (15)$$

where P is the confining pressure and V is the activation volume (e.g., Harrison et al. 1985; Giletti and Tullis 1977).

Episodic loss

Equation (12), the expression for the concentration distribution within a sphere, is of limited use in $^{40}\text{Ar}/^{39}\text{Ar}$ or U-Th/He dating as we lack the analytical resolution needed to directly image isotope distributions *in situ*. However, in cases where we can estimate the amount of uptake or loss into or from the solid, solutions relating the degree to which the system has approached equilibrium as a function of the Fourier number ($Dt/r^2 = Fo$) can be useful.

To obtain expressions for the fractional loss (or uptake), the concentration remaining after time t (determined by integrating the concentration distribution between $x = 0$ to $x = r$ at t) is subtracted from the initial uniform concentration, C_0 , and this remainder is then normalized to C_0 . This fraction represents the approach from zero loss ($f = 0$) at $t = 0$ to total equilibration at $t = \infty$. Thus fractional loss, f , is

$$f = \frac{M_0 - M_t}{M_0} = 1 - \frac{6}{\pi^2} \sum_{n=1}^{\infty} \frac{1}{n^2} \exp\left(\frac{-Dn^2\pi^2 t}{r^2}\right) \quad (16)$$

Graphical results of these equations for f vs. Dt/r^2 for spherical, cylindrical, and plane sheet geometries are shown in Figure 4; note for example, that a value of Dt/r^2 of 0.018 is required to produce a 40% fractional loss from a sphere.

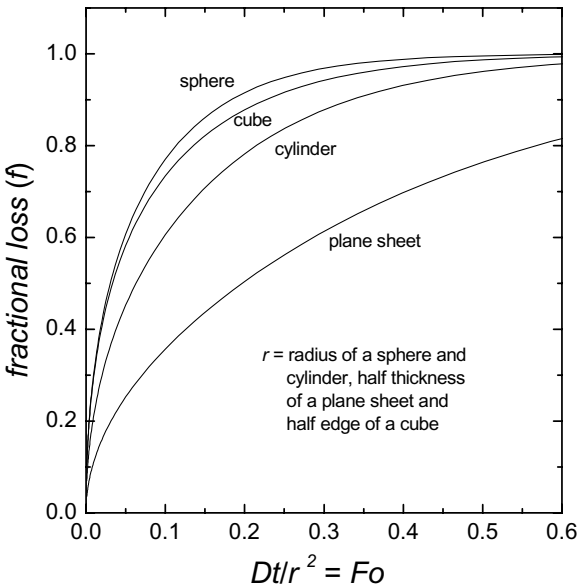


Figure 4. Relationship between fractional loss and the Fourier number (Dt/r^2) for spherical, cylindrical, plane sheet, and cubic geometries.

Coupling fractional loss equations with the Arrhenius relationship

Solutions of the diffusion equation in terms of fractional loss (f) yield expressions in terms of the Fourier number, Dt/r^2 ($= Fo$) (Fig. 4). Thus a numerical value of the Fo number can be calculated for any estimate of f . Substituting the Arrhenius relationship (Eqn. 13) into the definition of the Fo number yields an expression that relates fractional loss to peak temperature T in a square-pulse type thermal event of duration t :

$$\frac{E}{RT} = \ln\left(\frac{Fo^{-1}tD_0}{r^2}\right) \tag{17}$$

The principal limitation of this solution is that D lacks time dependence, restricting the equation to describing the geological uninteresting case of an isothermal history. However, by substituting:

$$\zeta = \int_0^t \left(\frac{D(t)}{r^2}\right) dt \tag{18}$$

for ($Fo^{-1} t$) we can then handle any arbitrary thermal history (Brandt 1974; Dodson 1975; Lovera et al. 1989). Understanding that this too-often unheralded substitution can be made is of critical importance in thermochronology. For example, assuming a temperature history of the form $t = 1/T$ permits Equation (17) to be integrated to yield an expression of the form

$$\frac{E}{RT_c} = \ln\left(\frac{A\tau D_0}{r^2}\right) \tag{19}$$

where A is a geometric constant and τ is a constant related to the cooling rate and activation energy (Dodson 1973). The parameter T_c is referred to as the closure temperature. It is in effect the characteristic temperature of retention associated with the age of the bulk geochronological system.

Calculation of age spectra resulting from episodic loss

While we are not yet able to clearly image $^{40}\text{Ar}/^{39}\text{Ar}$ distributions directly, the $^{40}\text{Ar}/^{39}\text{Ar}$ age spectrum method offers the potential to make observations at a fine spatial scale. Assuming the presence of a single site for Ar, synthetic $^{40}\text{Ar}/^{39}\text{Ar}$ age spectra based on diffusion from simple diffusion geometries can be constructed. In the case of radial diffusion from a sphere, the theoretical $^{40}\text{Ar}/^{39}\text{Ar}$ release pattern (Turner 1968) can be determined by evaluating the relative flux of ^{40}Ar with respect to ^{39}Ar .

For the case where: C_0 is the concentration of ^{40}Ar produced prior to outgassing, Δt_1 is duration of natural outgassing, $\Delta t'$ is the duration of laboratory outgassing, and C_{39} is the unit value of $^{39}\text{Ar}_K$ concentration, the $^{40}\text{Ar}/^{39}\text{Ar}$ ratio for any fractional loss of ^{39}Ar due to a laboratory heating $\Delta t'$, can be obtained by dividing the function that describes the $^{40}\text{Ar}^*$ flux from the sphere by the ^{39}Ar flux equation yielding:

$$\frac{^{40}\text{Ar}^*}{^{40}\text{Ar}_K} = \frac{C_0}{C_{39}} \left\{ \frac{\left[\sum_{n=1}^{\infty} \exp\left(\frac{-n^2\pi^2 D(\Delta t_1 + \Delta t')}{r^2}\right) \right]}{\left[\sum_{n=1}^{\infty} \exp\left(\frac{-n^2\pi^2 D(\Delta t')}{r^2}\right) \right]} \right\} \tag{20}$$

Synthetic $^{40}\text{Ar}/^{39}\text{Ar}$ ratios derived from this equation corresponding to 60 and 80% loss are shown in Figure 5 plotted against cumulative % ^{39}Ar . Also plotted in Figure 5 are theoretical age spectra for an infinite cylinder geometry.

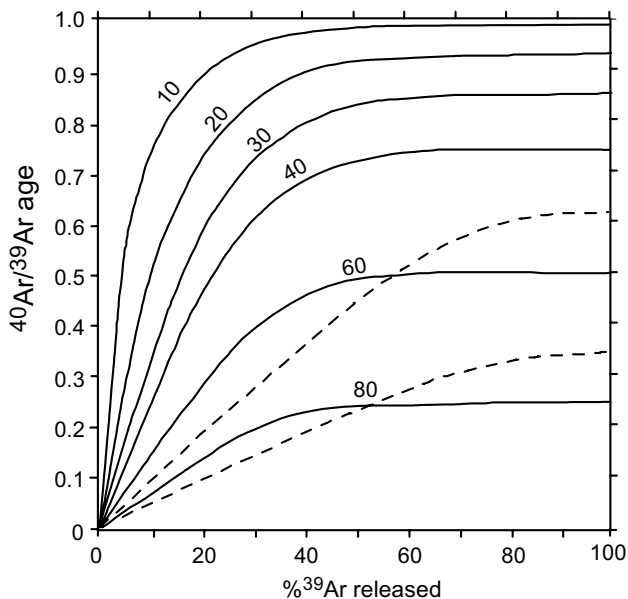


Figure 5. Theoretical $^{40}\text{Ar}/^{39}\text{Ar}$ age spectra for a sample of plane sheet geometry (solid lines) that has been outgassed today by 10, 20, 30, 40, 60, and 80% of $^{40}\text{Ar}^*$ present. For comparison, curves for 60 and 80% loss from spheres of uniform radius are shown as dashed lines.

The basis of this model can be seen in Figure 4. Note that the flux of ^{40}Ar or ^{39}Ar for any value of Dt/r^2 is given by the tangent to the curve. Because of the pronounced curvature of the function representing the sphere (due to the center of mass of the gas being closer to the diffusion boundary compared to the sheet model), a sample that has experienced even minor ^{40}Ar loss will not reach a uniform $^{40}\text{Ar}/^{39}\text{Ar}$ value until very late in the degassing. This is because even the small offset in Dt/r^2 between the ^{40}Ar and ^{39}Ar distributions places the ^{40}Ar gradient well up the steeply convex curve thus preventing the two tangents from becoming coincident until the sample is essentially outgassed. In contrast, the more linear nature of the plane sheet geometry curve allows the ^{40}Ar and ^{39}Ar gradients to rapidly reach a common value.

Closure temperature

Introduction. In the previous section, an expression was derived relating the Arrhenius relationship with solutions for fractional loss (for a constant D) to yield an expression that relates temperature and heating duration to the degree of isotopic equilibration (Eqn. 17). Of far greater importance is the case in which a sample experiences a complex thermal history, possibly involving heating as well as cooling, during which the daughter product is continually produced by radioactive decay and lost by diffusion. Although a closure temperature is only relevant to samples which that monotonically cooled from high to low temperatures, this condition holds for many samples, and in addition, closure temperature serves as a useful shorthand for describing the retentivity of a system.

Solutions for time-dependent D . Recall that by linking the dimensionless parameter Fo ($\equiv Dt/r^2$) obtained from the fractional loss expressions with the Arrhenius equation yielded a relationship (Eqn. 17) from which the maximum temperature of a square pulse thermal history could be calculated. Although this is of little geological utility, this simple expression does embody the basic form of the thermochronological relationship in that a characteristic temperature of the system is related to the diffusivity and time. The principal limitation of this relationship is that D lacks time dependence, restricting the equation to describing only a square-pulse thermal history. However, by substituting a time-varying diffusion coefficient defined as

$$\zeta = \int_0^t \left(\frac{D(T)}{r^2} \right) dt \quad (21)$$

into the diffusion equation modified to account for radiogenic ingrowth, then any arbitrarily thermal history can be evaluated yielding an equation of the form:

$$\frac{E}{RT} = \ln \left(\frac{A\tau D_0}{r^2} \right) \quad (22)$$

where A is a constant related to the geometry of diffusion (e.g., radial diffusion in a sphere) and the nature of the thermal history, τ is a function related to the form of the integrated thermal history, and T is the characteristic temperature of the system. For example, by assuming that the temperature history proceeds linearly in $1/t$, Equation (21) can be integrated to yield a simple relationship for τ that in turn permits a “closure temperature” to be calculated.

Monotonic cooling. Minerals originating at deep crustal levels undergo a transition during slow cooling from temperatures that are sufficiently high that the daughter escapes as fast as it is formed, to temperatures sufficiently low that diffusion is negligible and the retention of radiogenic isotopes by the mineral can be thought of as complete. Between these two states there is a continuous transition over which accumulation eventually balances loss, then exceeds it. Figure 6 (Dodson 1973) shows how a calculated age in this situation relates to the transition interval—the apparent age is the extrapolation of the total accumulation part of the curve to the time axis, which implicitly corresponds to an apparent temperature at which the bulk system became closed. In spite of the fact that closure does not occur at this time, the prior accumulation and subsequent loss balance to give thermal significance to the apparent age. Thus the general problem of isotopic closure during slow cooling is to quantify the shifting balance between accumulation and loss of daughter product. Assuming that a cooling history proceeds linearly in $1/T$, the decrease in the diffusion coefficient has the form of a simple exponential decay (Dodson 1973) with a time constant, τ , which corresponds to the time taken for D to diminish by a factor e^{-1} (i.e., to drop to 37% of its previous value). Thus from the Arrhenius relationship we can write

$$D = D_0 \exp \left(-\frac{E}{RT_0} - \frac{t}{\tau} \right) = D(0) \exp \left(-\frac{t}{\tau} \right) \quad (23)$$

where T_0 and $D(0)$ are the initial temperature and diffusion coefficient, respectively, at time $t = 0$. For example, when t corresponds to twice the time constant, the exponential coefficient

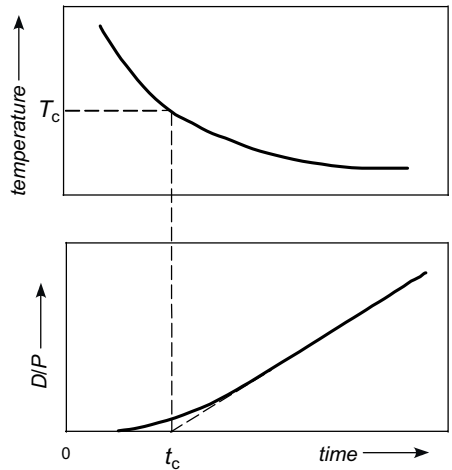


Figure 6. Diagrammatic depiction of closure model, where T_c is closure temperature and t_c is mineral age. During slow cooling from high temperature, the daughter to parent ratio (D/P) passes from a completely open state (i.e., $D/P = 0$) through a zone of partial accumulation, shown by the curved portion of the curve in the lower diagram, until the temperature is sufficiently low that diffusion loss ceases and the D/P ratio grows at a constant rate with time.

reduces the initial diffusivity to 14% of its original value. Note from Equation (23) that

$$\tau = \frac{R}{E dT^{-1}/dt} = \frac{RT^2}{E dT/dt} \quad (24)$$

This relationship holds provided that the cooling interval is short with respect to the half-life of the decay system used.

The exponential decay of the loss coefficient with time, a consequence of the form of the Arrhenius law, allows for a closed mathematical solution to the diffusion problem. Dodson (1973) derived a general solution of the accumulation–diffusion–cooling equation for a single diffusion length scale using appropriate substitutions and variable boundary conditions that reduced the problem to an equation identical to Fick’s Second Law. This equation can then be solved using general infinite series solutions (Carslaw and Jaeger 1959) for sphere, cylinder, and plane sheet geometries yielding expressions for the concentration distributions. Dodson (1973) also evaluated the coefficients which reduce these expressions to a single characteristic temperature he called the closure temperature (T_c) and provided two heuristic examples to illustrate the nature of the closure concept.

Below we show a non-rigorous calculation to illustrate how linking linear cooling in $1/T$ with diffusive loss via the Arrhenius relationship can derive the general form of the closure equation.

Simplified derivation of the closure temperature equation. Consider the cooling history shown in Figure 6 in which $1/T$ increases linearly. Assuming for the moment that the transition between open and closed system behavior occurs over the relatively narrow temperature interval from T_1 to T_2 (due to the strong temperature dependence of D), we can write two Arrhenius equations:

$$D_1 = D_0 \exp\left(-\frac{E}{RT_1}\right) \quad (25)$$

$$D_2 = D_0 \exp\left(-\frac{E}{RT_2}\right) \quad (26)$$

Dividing (26) by (25) yields

$$\frac{D_1}{D_2} = \exp\left[\left(-\frac{E}{R}\right)\left(\frac{1}{T_2} - \frac{1}{T_1}\right)\right] \quad (27)$$

Thus for a drop in diffusivity from T_1 to T_2 of a factor of e^{-1} ,

$$\frac{D_1}{D_2} = \frac{E}{R}\left(\frac{1}{T_2} - \frac{1}{T_1}\right) = 1 \quad (28)$$

But because $(T_2^{-1} - T_1^{-1}) \approx (\Delta T/T^2) = \dot{T}\Delta t/T^2$ (where \dot{T} is cooling rate), Equation (28) becomes

$$\frac{E \Delta T}{R T^2} \approx 1 \approx \frac{E \dot{T} \Delta t}{R T^2} \quad (29)$$

Recall that fractional loss from a sphere of radius r is associated with a specific value of Dt/r^2 . If we arbitrarily state that closure occurs at $Dt/r^2 = 1/A$ and substitute the Arrhenius relationship for D , then the bulk closure temperature of a mineral is given by:

$$\frac{E}{RT_c} = \ln \left(\frac{ART_c^2 D_0 / r^2}{E dT/dt} \right) \quad (30)$$

Despite the highly oversimplified nature of this derivation, it leads to the form of the closure equation. For the rigorous solution, the values for the geometric constant A can be evaluated and correspond to 55 for the sphere, 27 for the cylinder, and 8.7 for the plane sheet (Dodson 1973). Note that in the spherical case, a value of $A = 55$ corresponds to $Dt/r^2 = 0.018$ which in turn translates to a fractional loss of about 40%.

Note that Equation (30) is iterative in T_c . That is, a trial value inserted into the argument of the logarithm will return a second-order estimate of T_c . Because the logarithm dampens sensitivity to variations in the iterative process, this loop converges rapidly, usually in two iterations.

Assumptions of the closure temperature model. The closure temperature model (Eqn. 30) applies only in those cases where either the simplifying assumptions are met or the results are insensitive to violations of these assumptions. In the case of the slow-cooling model, the time constant (over which the diffusivity drops by a factor e^{-1}) must be much greater than the initial value of the characteristic diffusion time, $r^2/D(0)$. In other words, diffusion must be initially so rapid that the daughter product is not retained on a timescale equivalent to τ . Although the assumption of linear cooling in $1/T$ was adopted in order to make the mathematical solution tractable, a calculated closure temperature is generally highly insensitive to the form of the cooling history (Lovera et al. 1989). Other obvious violations of model interpretations include the presence of excess daughter product due to failure of the infinite reservoir assumption, subsequent open-system behavior, and mineral recrystallization. To expand on this latter point, should the mineral of interest form below the closure temperature, for example, during low grade metamorphism, then the closure model is no longer a valid description of the daughter retention history. Similarly, if cooling is accompanied by differential stress resulting in recrystallization, then the likelihood of diffusion being the rate-limiting daughter product transport mechanism during such structural reconstitution is remote.

Partial retention zone. The transitional interval of temperature (and for cooling geologic systems, time) that is implicit in closure theory finds real expression in crustal rocks. At Earth's surface temperature, all thermochronological systems will be effectively closed, and at lower-crustal depths and temperatures, all of the commonly used minerals used in thermochronometry will be completely open. Clearly with increasing depth and therefore temperature there will be a gradual transition for each system from closed to open behavior. This transition has been observed in deep boreholes, quite commonly for the less retentive systems such as fission-tracks in apatite and zircon (e.g., Naeser and Forbes 1976), but also in other minerals in deeper boreholes like the KTB hole or in exhumed crustal blocks (e.g., Warnock and Zeitler 1998; Stockli and Farley 2004). This transitional interval is referred to the "partial retention zone" or PRZ (Wolf et al. 1998); in fission-track dating the interval is referred to as the "partial annealing zone" or PAZ (Gleadow and Fitz Gerald 1987).

The exact nature of the PRZ depends on local geological conditions and the local tectonic history. In an active, steady-state orogen for example, where erosional exhumation is causing cooling of the crust, the crustal profile of mineral ages will be under the control of the rock uplift which is moving samples through the PRZ. In contrast, in a stable crustal column beneath, say, a craton, samples at various depths are in effect experiencing a prolonged isothermal heating in which daughter-isotope production and diffusional loss trade off to varying degrees, creating potentially large gradients in mineral age with depth. Figure 7 illustrates several forms that the PRZ might take. The accumulation of Ar or He in samples that were stagnant in the PRZ or took a complex path through has been modeled in most laboratories using numerical methods

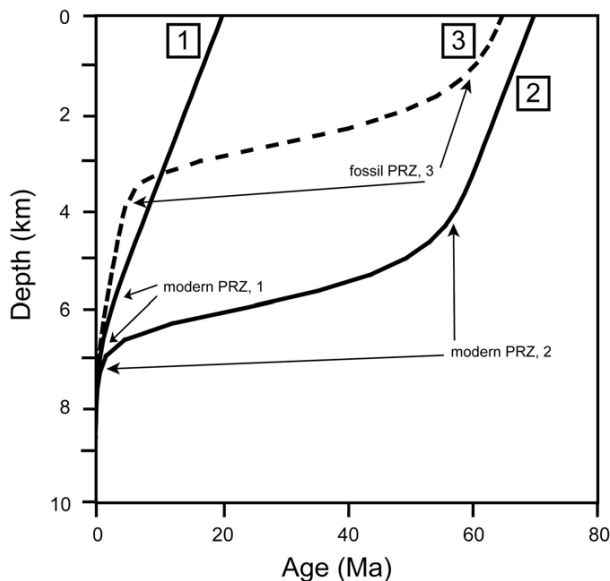


Figure 7. Schematic representation of “partial retention zone.” Solid curves show age profile in crust under conditions of continuous erosional cooling at orogenic rates (c1, at left) and after erosional cooling followed by a prolonged interval of stable conditions without erosion or burial (c2, right). Dashed curve (c3) shows crustal age profile after an modest pulse of uplift and erosion is superimposed on case c2. Approximate locations of modern and “fossil” PRZs are also shown.

that account for the general case of radiogenic accumulation and diffusive loss of daughter product (e.g., Wolf et al. 1998; Dunai 2005; Harrison et al. 2005; Ketcham 2005).

In certain circumstances, the PRZ has a sufficiently distinctive form that it can serve as an important marker in tectonic studies, something that has been widely exploited in low-temperature thermochronology in particular, using fission-track dating of apatite, and more recently U-Th/He dating of apatite and zircon (e.g. Stockli et al. 2000). Specifically, if a region has been tectonically stable and then experiences a pulse of rock uplift, it can be possible to identify a “fossil” PRZ in the pattern of ages with structural depth, providing information about both the timing and amount of exhumation (Fig. 7).

It is also very important to keep in mind that thermochronometers that have cooled through the PRZ will preserve an internal record of their passage in their daughter-product concentration profiles. Such “closure profiles” (Dodson 1986) can be inverted to provide a record of the relevant segment of the sample’s time-temperature history, provided this profile can be sampled by either indirect means such as $^{40}\text{Ar}/^{39}\text{Ar}$ or $^4\text{He}/^3\text{He}$ stepheating (Harrison et al. 2005; Shuster and Farley 2005) or direct sampling by direct means such as depth profiling by ion probe (e.g. Harrison et al. 2005).

EXPERIMENTAL DETERMINATION OF DIFFUSION PARAMETERS

Calculation of diffusion coefficients from bulk loss experiments

Because we are not able to directly observe natural $^{40}\text{Ar}/^{39}\text{Ar}$ or ^4He diffusion profiles, we must assess diffusion behavior by estimating the amount of uptake or loss. One commonly

used approach to measure diffusion of noble gases in natural materials is to measure the fractional approach toward equilibration of the radiogenic daughter resulting from a controlled heating experiment.

Approximations for fractional loss (f) from a sphere as a function of Dt/r^2 can be written (Fechtig and Kalbitzer 1966) in terms of the diffusion coefficient, D/r^2 . They are:

$$\frac{D}{r^2} = \begin{cases} \frac{1}{\pi^2 t} \left(2\pi - \frac{\pi^2}{3} f - 2\pi \sqrt{1 - \frac{\pi}{3} f} \right) & \text{for } f < 0.85 \\ \frac{1}{\pi^2 t} \ln \left[\frac{\pi^2}{6} (1-f) \right] & \text{for } f > 0.85 \end{cases} \quad (31)$$

In cases where r is the measured particle size, or can be inferred from experiment, a unique value for D can be determined.

Choosing an appropriate diffusion model for a mineral of complex geometry may not be immediately obvious. As an example, consider the case of biotite. Since diffusion in biotite proceeds much more rapidly parallel to the cleavage compared with perpendicular, an infinite cylinder may be an appropriate model despite the fact that mica is a sheet-like mineral. Planar structures such as perthite lamellae in alkali feldspar can be satisfactorily described as a plane sheet if the lamellar boundaries define the effective diffusion dimension.

Calculation of Ar and He diffusion coefficients from step-heating results

If we make the assumption that the diffusion mechanisms and boundaries that define Ar and He retentivity in nature are the same as those that control degassing during laboratory heating, we can also extract model diffusion coefficients (D/r^2) from stepwise heating of irradiated samples. Because the reactor-produced ^{39}Ar is distributed in a similar fashion to ^{40}K (which is broadly uniform within K-feldspars), it is preferable to use ^{39}Ar for this purpose as the concentration distribution of ^{40}Ar from slowly cooled samples is unknown. In the case of helium, until recently there has been no real choice but to use radiogenic ^4He as measured and, depending on the nature of the sample, either assume a uniform distribution, or attempt a workaround that assumes that there has been He loss or slow cooling sufficient to produce a concentration gradient, with diffusion calculations for later steps being relatively insensitive to the details of this assumption.

For the m^{th} laboratory heating step, $\log(D/r^2)$ can be written as (Lovera et al. 1997)

$$\log \left(\frac{D}{r^2} \right)_m = \log \frac{\Delta \zeta_m^*}{\Delta t_m} = \log \frac{\zeta_m^* - \zeta_{m-1}^*}{\Delta t_m} \quad (32)$$

where ζ_m is obtained from inversion of the approximate expressions for the cumulative fractions of ^{39}Ar or ^4He released. For the case of a plane sheet, $\Delta \zeta_m^*$ is

$$\Delta \zeta_m^* = \begin{cases} \frac{\pi}{4} (f_m^2 - f_{m-1}^2) & \text{for } f_m \leq 0.6 \\ -\alpha_1^{-2} \ln \left[\frac{(1-f_m)}{(1-f_{m-1})} \right] & \text{for } f_m > 0.6 \end{cases} \quad (33)$$

A potential limitation of this approach is that errors introduced at any step m are propagated into subsequent steps. An expression for the propagation of errors in calculation of diffusion coefficients from step heating data is given in Lovera et al. (1997).

Experimental criteria

The requirements of a diffusion study vary depending on the nature of the experiment, but two criteria must be met in all cases: the mineral must remain stable throughout the duration of the experiment and the initial distribution of the diffusing substance must be known. In the specific case of bulk-loss type experiments (e.g., Giletti 1974), several other factors must be known including the shape and effective diffusion length scale of the particles in the aggregate. For purposes of interpretation, diffusion experiments should be designed to address questions regarding chemical vs. tracer diffusion or wet vs. dry conditions. Recrystallization and incongruent dissolution during annealing are concerns that must be evaluated as are possible radiation-induced effects for $^{40}\text{Ar}/^{39}\text{Ar}$ or $^4\text{He}/^3\text{He}$ experiments.

Laboratory diffusion studies - helium

General observations. Studies conducted to date on He diffusion in apatite, zircon, and titanite all suggest that in these accessory minerals, the effective diffusion radius seems to be the physical grain size. All of these three phases show artifacts in their diffusion behavior in the form of non-linearities on their Arrhenius plots, with apatite being the best behaved at the more geologically relevant lower temperatures. In all cases, laboratory diffusion behavior under vacuum seems to be consistent with field calibrations, comparisons to one another, and comparisons to other thermochronometers. Shuster et al. (2003), in conducting their initial work on using proton-induced ^3He as a means of studying He diffusion, made the interesting finding that ^3He and ^4He seem to diffuse at very similar rates, despite the substantial relative difference in their masses. They speculate that the absence of the expected mass dependence of He diffusivity may be indicative of the diffusion mechanism in operation in apatite, with a process like diffusion of lattice defects being the controlling factor.

Apatite. Studies of Durango apatite indicate that He diffusion occurs via a thermally-activated volume diffusion process in the temperature region 100° to 300 °C with an activation parameters of $E = 32.9 \pm 1.6$ kcal/mol and $D_0 = 50$ cm²/s (Farley 2000). D_0/a^2 varies with grain size indicating that the grain size defines the diffusion domain (Farley 2000). These parameters translate into a closure temperature of 70 °C for apatites with a ca. 100 μm diffusion radius at a cooling rate of ca. 10 °C/Ma.

Zircon. Reiners et al. (2002) found that He release from zircon is complex. Temperature cycling experiments suggest that either zircon contains diffusion domains smaller than the physical grain size, or that annealing of radiation damage during the diffusion experiment was altering the diffusion properties of the zircon (Reiners 2005). They suggest a minimum activation energy for geological relevant ^4He diffusion of about 44 kcal/mol, and a 10 °C/m.y. closure temperature for typical zircons of about 190 °C. This estimate was supported by comparisons between K-feldspar-derived cooling histories and zircon helium ages, as well as further diffusion experiments (Reiners et al. 2003). These more recent data suggest activation energies of around 40 kcal/mol for portions of the low-temperature gas release, equivalent to closure temperatures of between 170 and 190 °C which show good concordance with the K-feldspar data (10 °C/m.y., 60 μm crystal radius).

Titanite. Reiners et al. (1999) examined He diffusion in titanite. Despite some non-linearity in diffusion behavior early in gas release, overall, He diffusion in titanite seems well-behaved, with much of the gas release following a linear Arrhenius relationship having an activation energy of ~45 kcal/mol. For the samples studied, the diffusion data equate to closure temperatures of about 190 to 220 °C (200 to 800 μm crystal radius, 10 °C/m.y.). In their study of titanites taken from the KTB deep borehole, Stockli and Farley (2004) found that their measured ages agreed very well with predictions for retentivity made from the diffusion data.

Laboratory diffusion studies - argon

Biotite-phlogopite. Using the bulk loss approach, Gilletti (1974) measured Ar diffusion from phlogopite (Ann₄) under hydrothermal conditions in the temperature range 900–600 °C and reported Arrhenius parameters of $E = 57.9 \pm 2.6$ kcal/mol and $D_0 = 0.75^{+1.7}_{-0.52}$ cm²/s. Using a similar experimental method, but under controlled oxygen fugacity conditions, Harrison et al. (1985) measured Ar diffusion from the Cooma biotite (Ann₅₆) in the temperature range 750–600 °C. For grain sizes less than 202 μm, they found $E = 47.0 \pm 2.1$ kcal/mol, $D_0 = 0.077^{+0.21}_{-0.06}$ cm²/s. Experiments at 14 kbar indicated an activation volume of 14 cm³/mol.

The fact that the 202 μm radius data plotted above the other data was attributed to the intrinsic effective diffusion radius being smaller than the measured grain radius. If so, this implies an *effective* diffusion radius of ~150 μm for this material, similar to estimates inferred from geological studies (e.g., Wright et al. 1991). Note that inferences from *in situ* laser probe studies that the characteristic Ar diffusion dimension is equivalent to grain size can be incorrect due to both low spatial resolution and the fact that the effective diffusive lengthscale is not equivalent to the largest domain size observed in a crystal (see Grove and Harrison 1996).

Grove and Harrison (1996) revisited the Cooma biotite and obtained $E = 45 \pm 3$ kcal/mol and $D_0 = 0.015^{+0.022}_{-0.005}$ cm²/sec, both values within 1σ of those previously obtained. Combining the two data sets yields an $E = 47.1 \pm 1.5$ kcal/mol and $D_0 = 0.075^{+0.049}_{-0.021}$ cm²/sec (Fig. 8). They also performed bulk loss experiments using an iron-rich biotite (Ann₇₁) which yielded $E = 50.5 \pm 2.2$ kcal/mol and a D_0 of $0.40^{+0.96}_{-0.28}$ cm²/sec—virtually indistinguishable from the Cooma biotite result.

Using an empirical diffusion model (Dowty 1980; Fortier and Gilletti 1989) to predict relationships between Ar diffusivity and chemistry, Grove (1993) identified composition controls on Ar diffusion in the biotite-phlogopite series. Specifically, Ar diffusivities are 1) enhanced by replacement of Mg²⁺ by Fe²⁺; (2) lowered by incorporation of Al(VI) and/or Fe³⁺ into the octahedral sheet; and (3) significantly lowered by replacement of the hydroxyl group by halogens.

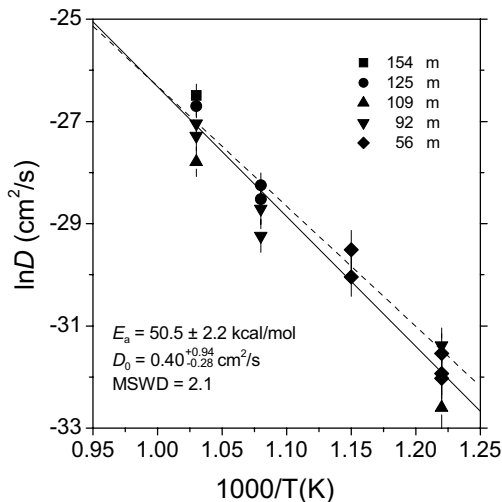


Figure 8. Arrhenius plot showing argon diffusion results for iron-rich [Fe/(Fe + Mg) = 71] Fe-mica from Grove and Harrison (1996). The composite line for the Cooma biotite is shown by the dashed line.

K-feldspar. Foland (1974) undertook an Ar diffusion study of a homogeneous orthoclase (Benson Mines) using hydrothermal and vacuum heating. These data yielded an $E = 43.8 \pm 1.0$ kcal/mol and $D_0 = 0.0098_{-0.0037}^{+0.0066}$ cm²/s and revealed that ⁴⁰Ar loss from alkali feldspar proceeds at the same rate whether heated in vacuum or under water pressure. Numerous vacuum step heating studies of irradiated K-feldspars have been undertaken as a by-product of ⁴⁰Ar/³⁹Ar dating (e.g., Berger and York 1981). Results of these experiments generally yield an initially linear array that was similar to the E obtained by Foland (1974). However, this simple Arrhenian behavior breaks down at higher temperatures yielding complex patterns. This behavior of the Arrhenius plot is now understood to result from basement K-feldspars typically containing a discrete distribution of diffusion length scales (Lovera et al. 1991).

The approach of using the vacuum step heating approach to establish argon diffusion behavior in K-feldspars was well documented by Lovera et al. (1997) who developed a large data base of analyzed samples. They focused on the low-temperature data which typically yield a linear Arrhenius relationship and statistically analyzed the results using an automated routine with a uniform set of selection criteria (Fig. 9). In general, they found that the propagated uncertainties in the calculation of $\log(D/r^2)$ from step heating data amount to only ± 0.05 log units (in s⁻¹). K-feldspars measured using a consistent extraction schedule (i.e., duplicate isothermal steps from 450–500 °C) yield Arrhenius plots with $\log(D/r^2)$ values that vary by less than two orders of magnitude at any given temperature.

Muscovite. The relatively narrow pressure-temperature field of stability of muscovite and Ar diffusion kinetics severely limits the experimental determination of argon diffusion to between 700 °C and 600 °C. Robbins (1972) undertook a hydrothermal diffusion study of muscovite and calculated Arrhenius parameters for his results using both an infinite cylinder and plane sheet model. A reasonably good fit of all data could be made with the plane sheet model yielding $E = 40$ kcal/mol and a $D_0 = 6 \times 10^{-7}$ cm²/s, although an equivalent argument could be

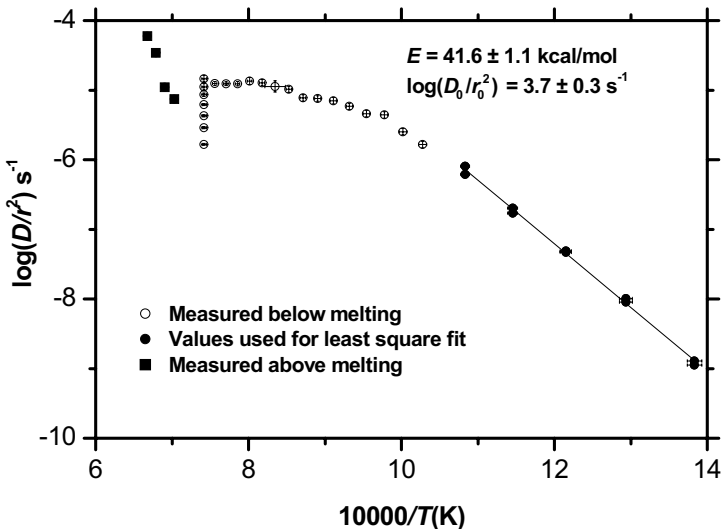


Figure 9. Arrhenius plot for a K-feldspar sample 93-NG-17 illustrating the method to calculate E and $\log(D_0/r_0^2)$. D/r^2 values are indicated by filled symbols and the solid line represents a weighted, least squares fit to these data.

made for the infinite cylinder calculation with a similar activation energy but a frequency factor some 500 times larger. Hames and Bowring (1994) re-evaluated Robbins (1972) results and preferred an infinite cylinder model with $E = 43 \pm 9$ kcal/mol and $\log D_0 = -3.4 \pm 2$ (cm^2/s). Lister and Baldwin (1996) instead argued for a sheet geometry with a characteristic thickness of ~ 12 μm for Robbins (1972) data.

Hornblende. Harrison (1981) used the bulk approach to examine the Ar diffusion behavior of two hornblende samples with Mg#’s of 0.72 and 0.36 in the temperature range 900–750 °C. The combined results defined a line of $E = 66 \pm 4$ kcal/mol and $D_0 = 0.06^{+0.4}_{-0.01}$ cm^2/s assuming a spherical model. Harrison et al. (1992) reported an additional diffusion measurement of the Mg-rich hornblende and obtained a somewhat lower value. Baldwin et al. (1990) further investigated the Fe-rich hornblende of Harrison (1981) and obtained results that were consistent with the earlier determined activation energy. They also hydrothermally treated two compositionally contrasting metamorphic amphiboles (Mg# of 0.71 and 0.43) containing complex exsolution structures. Results indicated that the effective diffusion lengthscale was substantially smaller than the measured particle size, probably reflecting the observed phyllosilicate intergrowths and/or exsolution lamellae that partition the hornblende crystals into smaller subdomains. No systematic dependence of argon diffusivity on Mg# has been yet established (Harrison 1981; Baldwin et al. 1990; Cosca and O’Nions 1994). The ionic porosity model (Fortier and Gilletti 1989; Dahl 1996) applied to the compositional dependence of argon retention in amphiboles predicts relatively small effects.

INTERPRETATION OF THERMOCHRONOLOGICAL DATA

It is beyond the scope of this chapter to explore modern approaches in interpreting thermochronological data. Instead we provide a few comments about the nature of such data, how they should be viewed, and what their current limitations are, echoing comments made by Reiners et al. (2005).

Heat transfer

Thermochronological data are inextricably linked to issues of how heat is transferred in the lithosphere and how various geodynamic processes alter the temperature potential field (Ehlers 2005). How exactly a thermochronological study is designed depends very much on the geologic context of the problem (Braun 2005; Gallagher et al. 2005). Interestingly and fortunately for the practitioner, both mass and heat conduction occur by diffusion, and so share a common mathematical description. However, in many cases geological problems are highly underdetermined when it comes to posing exact thermal solutions, and thermochronological data alone cannot make the difference even as they provide critical boundary conditions.

Very generally, higher-temperature systems will be easier to work with and interpret, as higher-temperatures in the crust will usually be less prone to locally complex temperature distributions and rapid changes in temperature. In contrast, at the very lowest temperatures at which thermochronology is currently applicable, below 100 °C, many processes beyond conductive heat transfer can become important (e.g., fluid flow), and topographic, structural, and lithologic factors all begin to play major roles in shaping the temperature field. In the shallow crust such phenomena as isotherm advection in three dimensions become significant in tectonically active regions.

Sampling considerations

In detail, what methods to use and how to distribute samples will depend entirely on the nature of the problem at hand. In general, geochronology has a legacy that emphasizes

precise analysis of small numbers of well-characterized samples. While we are certainly not opposed to precision and characterization, the thermal considerations we mentioned above do bring with them some demands. Faced with a complex temperature field that has evolved through time, sampling campaigns for thermochronology need to be wary of aliasing results through undersampling. Modern laboratories have greatly improved their capacities for sample throughput by means of automation and by reducing the amount of material that must be processed to obtain an analysis, but some compromise in method and precision might be required to meet the demands of an extended sampling campaign (e.g., opting for total-fusion rather than step-heating data for biotite samples, or substituting U-Th/He ages on zircon for detailed K-feldspar age spectra). Thinking about how seismic data are acquired and treated, in which multichannel sampling and procedures such as stacking enhance signal-to-noise ratios, we would argue that for many applications thermochronologists would benefit from an analogous approach.

Constraining power

Well-designed thermochronological studies and well-behaved samples can provide remarkably tight bounds on segments of thermal histories. However, it is important to keep in mind that at the other extreme, any single mineral age can be explained by myriad thermal histories, including monotonic cooling at varying rates, and all manner of resetting scenarios including prolonged thermal stagnation. To be most successful, thermochronological studies need to be carried out in conjunction with good structural, stratigraphic, and geochronological constraints.

Intercomparison and accuracy of thermochronological data

To date, there are no thermochronological standards available with which labs can compare results, either at the analytical level (e.g., diffusion data obtained from step-heating) or at a more derived level (e.g., complete thermal histories). In some cases, as in $^{40}\text{Ar}/^{39}\text{Ar}$ step-heating analysis of K-feldspar, segments of thermal histories can be determined that are probably precise and accurate to within 5–10 °C and well less than 1 m.y., assuming a well-behaved sample and a well-calibrated furnace. On the other hand, for many other mineral systems, much of our knowledge about their behavior comes from comparisons to other thermochronometers, diffusion data are scanty, and what diffusion data are available are frequently applied to unknowns based on mere assumptions about similarities in diffusion kinetics. Thus, determinations of parameters like cooling rates using “mineral pairs” will be fraught with pitfalls, given the assumptions and absolute uncertainties involved, and there is a clear need for more systematic and comprehensive studies of diffusion kinetics in minerals of importance.

CONCLUDING REMARKS

The fundamental nature of noble gas decay systems (i.e., chemically inert daughter products) leads to a high degree of predictability of closure temperature with a minimum of assumptions regarding initial non-radiogenic components. Similarities in the manner in which we can treat diffusive loss of daughter product from K-Ar and U-Th/He decay make it convenient for us to review the underlying theory of thermochronology using these two systems as exemplars. The great versatility of K-Ar and U-Th/He thermochronometers, which provide geological temperature monitoring across the range from 500 °C to 60 °C, make them the most popular methods for extracting temperature-time histories from crustal rocks.

REFERENCES

- Baldwin SL, Harrison TM, Fitz Gerald JD (1990) Diffusion of ^{40}Ar in metamorphic hornblende. *Contrib Mineral Petrol* 105:691-703
- Baxter EF, DePaolo DJ, Renne PR (2002) Spatially correlated anomalous Ar-40/Ar-39 "age" variations in biotites about a lithologic contact near Simplon Pass, Switzerland: A mechanistic explanation for excess Ar. *Geochim Cosmochim Acta* 66:1067-1083
- Berger GW, York D (1981) Geothermometry from $^{40}\text{Ar}/^{39}\text{Ar}$ dating experiments. *Geochim Cosmochim Acta* 45:795-811
- Brandt SB (1974) A new approach to the determination of temperatures of intrusions from radiogenic argon loss in contact aureoles. *In: Geochemical Transport and Kinetics*. Hofmann AW, Giletti BJ, Yoder HS, Yund RA (eds), Carnegie Institute, Washington, Publication # 634, p 295-298
- Braun J (2005) Quantitative constraints on the rate of landform evolution derived from low-temperature thermochronology. *Rev Mineral Geochem* 58:351-374
- Carlsaw HS, Jaeger JC (1959). *Conduction of heat in solids*, 2nd ed. Clarendon, Oxford.
- Chopin C, Maluski H (1980) $^{40}\text{Ar}/^{39}\text{Ar}$ dating of high-pressure metamorphic micas from the Gran Paradiso area (Western Alps) – Evidence against the blocking temperature concept. *Contrib Mineral Petrol* 74: 109-122
- Cosca MA, O'Nions RK (1994) A re-examination of the influence of composition on argon retentivity in metamorphic calcic amphiboles. *Chem Geol* 112:39-56
- Crank J (1975) *The mathematics of diffusion*. Oxford University Press, Oxford
- Dahl PS (1996) The effects of composition on retentivity of argon and oxygen in hornblende and related amphiboles: a field-tested empirical model. *Geochim Cosmochim Acta* 60:3687-3700
- de Jong K (2003) Very fast exhumation of high-pressure metamorphic rocks with excess ^{40}Ar and inherited ^{87}Sr , Betic Cordillera, southern Spain. *Lithos* 70:91-110
- Dodson MH (1973) Closure temperature in cooling geochronological and petrological systems. *Contrib Mineral Petrol* 40:259-274
- Dodson MH (1975) Kinetic processes and thermal history of rocks. *Ann Rep Dir Dept Terr Magn Carnegie Inst Yearbook* 74, p 210-217
- Dodson MH (1986) Closure profiles in cooling systems. *In: Materials Science Forum*, Vol 7. Trans Tech Publications, Aedermannsdorf, Switzerland, p 145-153
- Dowty E (1980) Crystal-chemical factors affecting the mobility of ions in minerals. *Am Mineral* 65:174-182
- Dunai TJ (2005) Forward modeling and interpretation of (U-Th)/He ages. *Rev Mineral Geochem* 58:259-274
- Ehlers TA (2005) Crustal thermal processes and the interpretation of thermochronometer data. *Rev Mineral Geochem* 58:315-350
- Farley KA (2000) Helium diffusion from apatite: general behavior as illustrated by Duragno fluorapatite. *J Geophys Res* 105:2903-2914
- Farley KA, Reiners PW, Neno V (1999) An apparatus for measurement of noble gas diffusivities from minerals in vacuum. *Anal Chem* 71:2059-2061
- Farley KA, Wolf RA, Silver LT (1996) The effects of long alpha-stopping distances on (U-Th)/He dates. *Geochim Cosmochim Acta* 60:4223-4230
- Faure G (1977) *Principles of isotope geology*. Wiley, New York
- Fechtig H, Kalbitzer S (1966) The diffusion of argon in potassium-bearing solids. *In: Potassium-argon Dating*. Schaeffer OA, Zähringer J (eds) Springer-Verlag, New York, p 68-107
- Fick A (1855) Ueber diffusion. *Ann Phys Chem* 94:59-86
- Fitz Gerald JD, Harrison TM (1993) Argon diffusion domains in K-feldspar I: microstructures in MH-10. *Contrib Mineral Petrol* 113:367-380
- Foland KA (1974) ^{40}Ar diffusion in homogeneous orthoclase and an interpretation of Ar diffusion in K-feldspar. *Geochim Cosmochim Acta* 38:151-166
- Fortier SM, Giletti BJ (1989) An empirical model for predicting diffusion coefficients in silicate minerals. *Science* 245:1481-1484
- Gallagher K, Stephenson J, Brown R, Holmes C, Ballester P (2005) Exploiting 3D spatial sampling in inverse modeling of thermochronological data. *Rev Mineral Geochem* 58:375-387
- Giletti BJ (1974) Diffusion related to geochronology. *In: Geochemical Transport and Kinetics*. Hofmann AW, Giletti BJ, Yoder Jr. HS, Yund RA (eds), Carnegie Inst. of Wash. Publ. 634, p 61-76
- Giletti BJ, Tullis J (1977) Studies in diffusion. IV. Pressure dependence of Ar diffusion in phlogopite mica. *Earth Planet Sci Lett* 35:180-183
- Gleadow AJW, Fitzgerald PG (1987) Tectonic history and structure of the Transantarctic Mountains: new evidence from fission track dating in the Dry Valleys area of southern Victoria Land. *Earth Planet Sci Lett* 82:1-14
- Grove M, Harrison TM (1996) ^{40}Ar diffusion in Fe-rich biotite. *Am Mineral* 81: 940-951

- Grove M (1993) Thermal histories of southern California basement terranes. PhD dissertation, University of California, Los Angeles, CA
- Hames WE, Bowring SA (1994) An empirical evaluation of the argon diffusion geometry in muscovite. *Earth Planet Sci Lett* 124:161-167
- Harrison TM (1981) Diffusion of ^{40}Ar in hornblende. *Contrib Mineral Petrol* 78:324-331
- Harrison TM, McDougall I (1981) Excess ^{40}Ar in metamorphic rocks from Broken Hill, New South Wales: Implications of $^{40}\text{Ar}/^{39}\text{Ar}$ age spectra and the thermal history of the region. *Earth Planet Sci Lett* 55:123-149
- Harrison TM, Duncan I, McDougall I (1985) Diffusion of ^{40}Ar in biotite: temperature pressure and compositional effects. *Geochim Cosmochim Acta* 49:2461-2468
- Harrison TM, Heizler MT, Grove M, Wartho J (1992) Argon loss from hornblende. *EOS Trans Am Geophys Un* 73:362
- Harrison TM, Grove M, Lovera OM, Zeitler PK (2005) Continuous thermal histories from inversion of closure profiles. *Rev Mineral Geochem* 58:389-409
- Hourigan JK, Reiners PW, Brandon MT (2005) U-Th zonation dependent alpha-ejection in (U-Th)/He chronometry. *Geochim Cosmochim Acta* 69:3349-3365
- Huneke JC, Smith SP (1978) The realities of recoil: ^{39}Ar recoil out of small grains and anomalous age patterns in ^{39}Ar - ^{40}Ar dating. *Proc 7th Lunar Sci Conf* 1987-2008.
- Hurley PM (1954) The helium age method and the distribution and migration of helium in rocks. *In: Nuclear Geology*. Faul H (ed) Wiley, New York, p 301-329
- Ketcham RA (2005) Forward and inverse modeling of low-temperature thermochronometry data. *Rev Mineral Geochem* 58:275-314
- Lister GS, Baldwin SL (1996) Modelling the effect of arbitrary P-T-t histories on argon diffusion in minerals using the MacArgon program for the Apple Macintosh. *Tectonophysics* 253:83-109
- Lovera OM, Richter FM, Harrison TM (1989) $^{40}\text{Ar}/^{39}\text{Ar}$ geothermometry for slowly cooled samples having a distribution of diffusion domain sizes. *J Geophys Res* 94:17917-17935
- Lovera OM, Richter FM, Harrison TM (1991) Diffusion domains determined by ^{39}Ar release during step heating. *J Geophys Res* 96:2057-2069
- Lovera OM, Grove M, Harrison TM, Mahon KI (1997) Systematic analysis of K-feldspar $^{40}\text{Ar}/^{39}\text{Ar}$ step-heating results: I Significance of activation energy determinations. *Geochim Cosmochim Acta* 61:3171-3192
- Meesters AGCA, Dunai TJ (2002a) Solving the production-diffusion equation for finite diffusion domains of various shapes - Part I. Implications for low-temperature (U-Th)/He thermochronology. *Chem Geol* 186:333-344
- Meesters AGCA, Dunai TJ (2002b) Solving the production-diffusion equation for finite diffusion domains of various shapes - Part II. Application to cases with alpha-ejection and nonhomogeneous distribution of the source. *Chem Geol* 186:57-73
- McDougall I, Harrison TM (1999) *Geochronology and Thermochronology by the $^{40}\text{Ar}/^{39}\text{Ar}$ Method*. 2nd ed, Oxford University Press, New York
- Obradovich JD, Tatsumoto M, Manuel OK, Mehnert H, Domenick M, Wildman T (1982) K-Ar and K-Ca dating of sylvite from the late Permian Salado Formation New Mexico Implications regarding stability of evaporite minerals. *Fifth Int Conf Geochronol Cosmochronol Isotope Geol, Japan*, 283-284
- Pankhurst RJ, Moorbath S, Rex DC, Turner G (1973) Mineral age patterns in ca. 3700 my old rocks from West Greenland. *Earth Planet Sci Lett* 20:157-170
- Purdy JW, Jäger E (1976) K-Ar ages on rock-forming minerals from the Central Alps. *Mem Ist Geol Min Univ Padova* 30, 31 pp.
- Reiners PW (2005) Zircon (U-Th)/He thermochronometry. *Rev Mineral Geochem* 58:151-179
- Reiners PW, Ehlers TA, Zeitler PW (2005) Past, present, and future of thermochronology. *Rev Mineral Geochem* 58:1-18
- Reiners PW, Farley KA (1999) Helium diffusion and (U-Th)/He thermochronometry of titanite. *Geochim Cosmochim Acta* 63:3845-3859
- Reiners PW, Farley KA, Hickes HJ (2002) He diffusion and (U-Th)/He thermochronometry of zircon: Initial results from Fish Canyon Tuff and Gold Butte, Nevada, *Tectonophysics*, 349:297-308
- Reiners PW, Spell TL, Nicolescu S, Zanetti, KA (2004) Zircon (U-Th)/He thermochronometry: He diffusion and comparisons with $^{40}\text{Ar}/^{39}\text{Ar}$ dating, *Geochim Cosmochim Acta* 68:1857-1887
- Robbins GA (1972) Radiogenic argon diffusion in muscovite under hydrothermal conditions. MS thesis, Brown University, Providence RI
- Shuster DL, Farley KA (2003) $^4\text{He}/^3\text{He}$ thermochronometry. *Earth Planet Sci Lett* 217:1-17
- Shuster DL, Farley KA (2005) $^4\text{He}/^3\text{He}$ thermochronometry: theory, practice, and potential complications. *Rev Mineral Geochem* 58:181-203

- Shuster DL, Farley KA, Sistierson JM, Burnett DS (2003). Quantifying the diffusion kinetics and spatial distributions of radiogenic ^4He in minerals containing proton-induced ^3He . *Earth Planet Sci Lett* 217: 19-32
- Stockli DA, Farley KA (2004) Empirical constraints on the titanite (U-Th)/He partial retention zone from the KTB drill hole. *Chem Geol* 207:223-236
- Stockli DA, Farley KA, Dumitru TA (2000) Calibration of the (U-Th)/He thermochronometer on an exhumed normal fault block in the White Mountains, eastern California and western Nevada. *Geology* 28:983-986
- Strutt RJ (1908) The accumulation of helium in geological time. *Proc Roy Soc Lond A* 80:272-277
- Turner G (1968) The distribution of potassium and argon in chondrites. *In: Origin and Distribution of the Elements*. Ahrens LH (ed) Pergamon, London, p 387-398
- Turner G, Cadogan PH (1974) Possible effects of ^{39}Ar recoil in ^{40}Ar - ^{39}Ar dating. *Geochim Cosmochim Acta Suppl* 5 (Proceedings of the Fifth Lunar Science Conference), 1601-1615
- Warnock AC, Zeitler PK (1998) $^{40}\text{Ar}/^{39}\text{Ar}$ thermochronometry of K-feldspar from the KTB borehole, Germany. *Earth Planet Sci Lett* 158:67-79
- Wright N, Layer PW, York D (1991) New insights into thermal history from single grain $^{40}\text{Ar}/^{39}\text{Ar}$ analysis of biotite. *Earth Planet Sci Lett* 104:70-79
- Wolf RA, Farley KA, Kass DM (1998) Modeling of the temperature sensitivity of the apatite (U-Th)/He thermochronometer. *Chem Geol* 148:105-114
- Wolf RA, Farley KA, Silver LT (1996) Helium diffusion and low-temperature thermochronometry of apatite. *Geochim Cosmochim Acta* 60:4231-4240
- Zeitler PK, Herczig AL, McDougall I, Honda M (1987) U-Th-He dating of apatite: a potential thermochronometer. *Geochim Cosmochim Acta* 51:2865-2868